Heliyon 8 (2022) e10971

Contents lists available at ScienceDirect

Heliyon

journal homepage: www.cell.com/heliyon

Research article

Electrochemical response of solidification Cu^{2+} contaminated soil influenced by red mud/fly ash ratio

Wang Wen [a], Lijun Jia [b], Jun Xie [a], Wenjing Zhao [b], Huimin Feng [b], Dehua Cao [b], Funan Sun [a], Pengju Han [a], Xiaohong Bai [a], Bin He [a,*]

[a] College of Civil Engineering, Taiyuan University of Technology, Taiyuan 030024, China
[b] Shanxi Shan'an Lide Environmental Science and Technology Co., Ltd, Taiyuan 030032, China

ARTICLE INFO

Keywords:
Cu^{2+}-contaminated soil
Curing agent
Unconfined compressive strength
Electrochemical impedance spectroscopy
Microstructure

ABSTRACT

The main purpose of this work was to study a new method for evaluating the solidification of contaminated soil based on electrochemical impedance spectroscopy (EIS). To explore how the EIS parameters were affected by the pore structure and mesostructure of the cured system, the physical and mechanical properties, leaching toxicity, microstructure, and EIS of the stabilized contaminated soil were tested after 7, 28, 60, and 90 days of curing. Based on the EIS results, a physical and equivalent circuit model of the stabilized contaminated soil's impedance response was established to reveal the mechanism of binder-heavy metal ion-soil interaction. The results showed that as the red mud (RM)-fly ash (FA) mass ratio and curing age increased, the strength and structural compactness of the solidified body also increased. The best curing effect was achieved with an RM-FA mass ratio of 7:3 after curing for 90 days. The equivalent circuit model of the solidified body obtained by EIS was R_s (Q_1 (R_{ct1}W) Q_2R_{ct2}). The pore solution resistance R_s, solid-liquid interface ion transfer resistance Rct 1, and unconfined compressive strength (UCS) q_u all showed an increasing trend with increasing RM-FA mass ratio and increasing curing time. Fitting the model demonstrated that both R_s and R_{ct1} were closely correlated with the strength of the solidified bodies. These conclusions were further verified by scanning electron microscope (SEM) experiments. Overall, this work demonstrates that the strength characteristics of solidified bodies can be evaluated by EIS and reveals the microscopic mechanism of the solidification of Cu^{2+}-contaminated soil.

1. Introduction

The treatment of solid waste in China faces severe challenges such as high generation intensity, insufficient utilization, and the low added value of comprehensive utilization products due to China's energy structure and development stage. At present, solid waste stockpiles in China amount to 60 billion tons. Red mud (RM) and fly ash (FA) are two of the most significant industrial solid wastes due to their high discharge rate, high production intensity, low utilization rates and utilization levels, and high ecological and environmental security risks. RM is a strong alkaline solid waste produced during the production of alumina. The amount of RM generated in China from 2011 to 2018 according to the National Bureau of Statistics of China is shown in Figure 1. The comprehensive utilization rate of RM in China was only 4.29% in 2018. Moreover, China is still a major coal-producing country, leading to significant FA production. Figure 2 shows the distribution of China's industrial FA production in 2018. As can be seen, FA is the main solid waste discharged from thermal power plants. Currently, the resource utilization rate of FA is relatively high, and it is most widely used in construction materials. Cement, concrete, and bricks produced using FA have been used in large quantities in many actual projects (Kirgiz, 2018; Kumar and Kumar, 2013; Viyasun et al., 2021).

At the same time, heavy metal pollution in soils is also a serious global problem, with more than 20 million hectares of land around the world polluted by heavy metals such as Qu, Cd, Cr, Hg, Pb, Co, Cu, Ni, Zn, and Se (Liu et al., 2018). Soil pollution is particularly concentrated in the densely populated Yangtze River Delta, Pearl River Delta, and Southwest and Central South regions in China. The heavy metal copper, which is widely used in many industrial fields, is a widespread soil contaminant due to its significant use in long-term mining processes. Moreover, the content of copper ions in contaminated soil is several times to tens of times higher than that in original soil environments (Duan et al., 2016; Hu et al., 2019). Therefore, the remediation of heavy metal contaminated soil is an urgent problem that requires new soil management strategies to be solved.

* Corresponding author.
E-mail address: hebin@tyut.edu.cn (B. He).

https://doi.org/10.1016/j.heliyon.2022.e10971
Received 17 March 2022; Received in revised form 11 August 2022; Accepted 30 September 2022

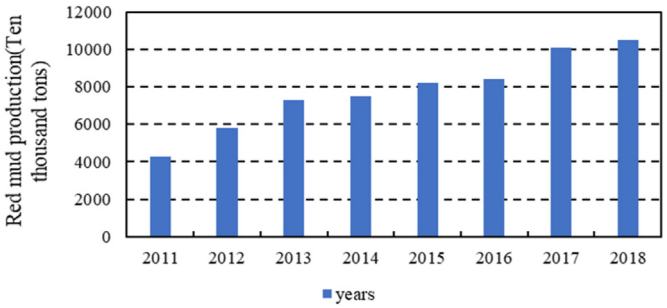

Figure 1. The amount of red mud produced in China from 2011 to 2018.

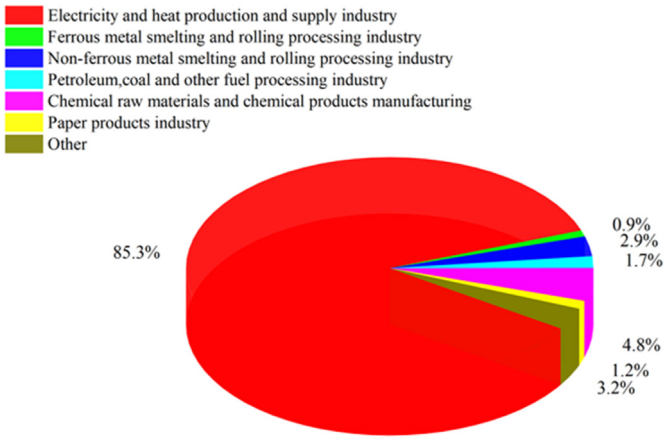

Figure 2. The distribution of fly ash production by industrial enterprises in 2018.

In recent years, some scholars have found that industrial solid waste can promote the solidification of heavy metals, and industrial waste residues such as RM, FA, coal slag, steel slag, and biochar have been modified for use in the solidification of heavy metal contaminated soil (Atanes et al., 2019; Cho et al., 2019; Derakhshan Nejad et al., 2018; Du et al., 2020; Gong et al., 2018; Goodarzi and Movahedrad, 2017; Hossain et al., 2020; Li et al., 2019; Tajudin et al., 2016; Xia et al., 2019; Yang et al., 2019; Wang et al., 2022) Among these waste residues, RM has been widely researched as a remediation agent for heavy metal contaminated soil (Hua et al., 2017). RM has been shown to reduce the migration of heavy metals in soil, affect the efficiency of solidifying Pb, Cd, Zn in contaminated soil, and improve the microbial characteristics in soil after solidification (Garau et al., 2007). FA is also widely used in the remediation of polluted soil. Some researchers have experimentally studied the solidification effect of lime, FA, and coal slag on heavy metals in tannery sludge. This study reported that solidified sludge blocks achieved relatively high strengths, even with low amounts of lime, FA, and coal slag. Moreover, the concentration of heavy metals leached from test blocks after curing treatment met the standard (Tian et al., 2011). Other studies have reported the long-term leachability, heavy metal transformation, and solidification mechanism of cement-cured Ni, Cu, Zn, Cd, and Pb polluted soil (Wang et al., 2015).

Investigating the strength characteristics of solidified soils requires convenient testing methods. Electrochemical impedance spectroscopy (EIS) is a non-destructive testing method that can be used to study the hardening mechanism of alkali-excited materials. Results have shown that electrochemical impedance parameters follow the same trend and strongly correlate with compressive strength (Fang et al., 2019; Zha et al., 2009, 2019). Moreover, traditional evaluation indices cannot characterize the internal dynamic response characteristics during the evolution of engineering properties during soil solidification (Liu et al., 2016; Zha et al., 2007, 2011). Thus, EIS shows good promise for investigating the compressive strength of solidified contaminated soils.

In summary, focusing on the frontier issues of solidification and stabilization of copper ion contaminated soil, this paper uses the common bulk solid wastes RM and FA along with a small amount of quicklime and cement as curing agents in a soil solidification process. Specifically, the electrochemical impedance characteristics of Cu^{2+}-contaminated soil are investigated during curing and remediation. Unconfined compressive strength (UCS) and EIS test methods are used to study the changes in compressive strength and the electrochemical impedance characteristics of three RM-FA mixture ratios aged for four different times. Combined with SEM analysis, the effect of RM and FA on the stabilization of copper ions in the soil samples are explored herein. These research results provide a theoretical basis for the comprehensive utilization of the common solid wastes RM and FA. Moreover, this work reports a new method for evaluating the solidification and repair of soil contaminated by copper ion, helping promote the green and sustainable development of society by improving the utilization of solid waste.

2. Materials and methods

2.1. Materials

The soil used in this experiment was 325 mesh commercial kaolin, which was a white powder. The chemical composition of the kaolin is shown in Table 1. RM was obtained from the Bayer process of an aluminum plant in Shanxi Province, China. The RM was crushed to 200 mesh prior to use. The chemical composition of the RM is shown in Table 1. FA was taken from a coal-fired thermal power plant in Shanxi Province, China, and the sulfur content of the FA was relatively high. The chemical composition of the FM is shown in Table 1. P.O.42.5 Ordinary Portland Cement was used, and the chemical composition of this cement is shown in Table 1. Analytical grade CaO was used as quicklime, and analytical grade $Cu(NO_3)_2{\cdot}3H_2O$ was used as the Cu pollution source.

2.2. Preparation of test samples

This work was divided into a pre-experiment and a formal experiment. In the pre-experiment, multiple raw material ratios were used to determine the amounts of cement and quicklime and the water-cement ratio for the formal experiment. The curing agent ratio was adjusted based on the time required for slurries to set, the difficulty of molding specimens, and economic considerations. Three different RM-FA ratios were selected for the formal experiment, and three parallel specimens were produced for each RM-FA ratio. Thus, 9 cured body specimens were prepared. Based on the amount of kaolin, the total amount of RM and FA was 35%, the copper ion concentration was 0.4%, the cement content was 7%, the CaO content was 3.5%, and the water-solid ratio was 0.45. The cured sample mixing ratio is shown in Table 2. Four curing times were investigated: 7 days, 28 days, 60 days, and 90 days.

According to the selected mixing ratio, the desired amounts of soil, copper nitrate, RM, FA, cement, quicklime, and water were weighed. First, the barrel and blades of a mortar mixer were wiped with a clean damp cloth. Next, the weighed soil and $Cu(NO_3)_2{\cdot}3H_2O$ were thoroughly mixed and evenly stirred to prepare a copper ion contaminated soil sample. The curing agent (the RM, FA, cement, and quicklime) was then poured into the mortar mixer with the prepared contaminated soil. This mixture was stirred for 1 min, then the specified amount of water was added. The wet slurry was then thoroughly mixed in the mortar mixer until it was uniform. Finally, this mixture was poured into a removable steel mold with dimensions of 70.7 mm × 70.7 mm × 70.7 mm. The slurry-filled mold was placed on a shaking table and vibrated for 2 min to allow the slurry to evenly and densely fill the mold, and excess slurry was scraped off. The surface of the mold was smoothed with a scraper, and the mold was then wrapped with a preservative film to prevent moisture evaporation from the specimen surface. Specimens were allowed to solidify in the molds for 24 ± 2 h. Then, the molds

Table 1. The main chemical composition of test materials.

	Al_2O_3	SiO_2	Fe_2O_3	CaO	MgO	K_2O	Na_2O	TiO_2	SO_3	S	Loss
Kaolin	27.06	57.53	0.28	0.084	0.89	5.29	0.18	0.04	-	-	1.57
Red mud	23.78	21.05	0.42	14.91	0.53	0.77	11.86	4.04	–	-	12.32
Fly ash	34.6	18.57	7.66	23.57	3.41	-	-	-	6.99	-	2.75
Cement	20.96	4.98	3.22	64.03	0.55	1.30	0.07	-	-	2.60	2.29

Table 2. Design of proportioning ratio of cured body specimen.

Numbering	kaolin/g	RM + FA/g	RM:FA	CaO/g	Cement/g	Cu^{2+}/g
1	100	35	3:7	3.5	7	0.4
2	100	35	5:5	3.5	7	0.4
3	100	35	7:3	3.5	7	0.4

were removed and the specimens were placed in a curing box set to a temperature of 20 ± 2 °C and a relative humidity of 90% or higher. After curing for 7 days, 28 days, 60 days, or 90 days, EIS and the UCS tests were both performed. After the end of the UCS test on the 90th day, the 90-day test specimens were pressed to failure. The broken fragments of these damaged specimens were investigated by SEM. These broken test pieces were cut and machined to a length of about 2 cm and a thickness of about 1 cm. The surfaces of these samples were smoothed with sandpaper, and surface dust was washed away with absolute ethanol. Finally, the samples were dried in an oven at 105 °C for 3 h until a constant weight was achieved.

2.3. Experimental procedures and methods

EIS and UCS tests were carried out on specimens with different RM-FA mass ratios and different curing times. A CS350 electrochemical workstation was used for EIS measurements. An EIS frequency range of 10^{-2}-10^{5} Hz and the linear logarithmic sweep mode were used. The amplitude of the applied sine wave was 10 mV. Impedance tests of the solidified body specimens were carried out by using the dual-electrode method. The dual electrodes were the working electrode and the auxiliary electrode. In each test, one side of a solidified body specimen was connected to the working electrode (WE) and placed on the test bench. The opposite side of the working electrode was connected to the auxiliary electrode (CE). Both test electrodes had copper endings. Copper was chosen due to its good conductivity and chemical inertness (Dong et al., 2016; Younsi et al., 2015). To ensure full contact between the test block and the electrodes, the copper electrode was covered with a glass sheet, and a steel block was placed on top of the glass sheet. This assembly was placed in a Faraday shielded box. EIS tests were performed after 7 days, 28 days, 60 days, and 90 days of curing, as shown in Figure 3. After the EIS tests, Nyquist and Bode plots of the cured bodies were obtained. The obtained electrochemical impedance spectra were analyzed by ZView and ZSimDemo, and an equivalent circuit model of the cured bodies was established. The electrochemical impedance parameters of the cured bodies were obtained, and the parameters were used to evaluate the curing effect of different RM-FA mass ratios.

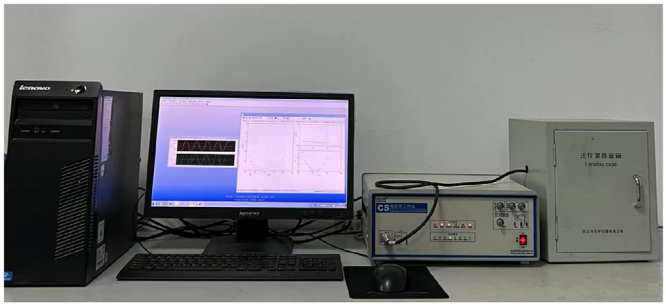

Figure 3. CS350 electrochemical workstation.

A UCS test was carried out after electrochemical measurements for each cured specimen. A Shimadzu AG-25TB universal testing machine was used for the UCS tests. A displacement of 0.03 mm s^{-1} was used until specimen failure, and the failure load was recorded (Zentar et al., 2021). The UCS of each specimen was calculated according to Eq. (1):

$$q_u = \frac{P}{A} \tag{1}$$

where q_u is the unconfined compressive strength of each specimen, P is the failure load, and A is the cross-sectional area of each specimen.

After the EIS and UCS tests on the 90th day, SEM was used to observe the microscopic morphology and internal structure of the three solidified body specimens cured for 90 days. A TM3000 desktop scanning electron microscope (Hitachi, Japan) was used. This instrument can magnify samples by 30–10000 times, and the moving range of microscopic samples in two directions is 17.5 mm. Prior to SEM analysis, each sample surface was gold-plated by an SBC-12 small ion sputtering instrument. A vacuum of 5–6 Pa and a plasma current of less than 10 mA were used for sputtering. The morphology of hydration products inside the solidified body specimens was observed and studied by SEM. This morphology was used to analyze the solidification effect as well as the effect of the RM-FA-cement-quicklime system on the copper ions.

3. Results and discussion

3.1. Electrochemical impedance characteristics of cured bodies under different RM-FA ratios

The electrochemical impedance spectra of the cured bodies produced with different RM-FA mass ratios at various ages are shown in Figure 4 (a-d). The Nyquist plots of all the solidified bodies exhibit arcs in the high-frequency region. These arcs are referred to as capacitive arcs, and their diameters are related to material compactness. The low-frequency regions of the Nyquist plots present slopes of about 45°, which is the diffusion slope of ion diffusion. This slope describes the transfer process of the diffused material—that is, the Warburg impedance (Casero et al., 2012; Huang, 2018; Qiu et al., 2017).

The capacitance arc diameters of the high-frequency region in the Nyquist plots increase with increasing RM-FA mass ratio. Under a low RM-FA mass ratio (less RM and more FA), the existence of a large amount of FA means that it is difficult to fully activate the FA. Thus, only a portion of this material reacts to form silicon-aluminum gel. Moreover, ion exchange reactions between Ca^{2+}/Cu^{2+} and Na^{+}/K^{+} that occur on the surface of RM only occur with difficulty due to the low amount of RM (Mahendran et al., 2013; Suo et al., 2021). Thus, fewer particle clusters are formed. The gel formed by the hydration reaction is therefore less connected to the solidified material. Consequently, the internal pores of the solidified body are larger, the material is not very dense, and charge transfer easily occurs. The electrochemical impedance spectra of the specimens produced with low RM-FA ratios exhibit small capacitance arc radii in the high-frequency regions of their

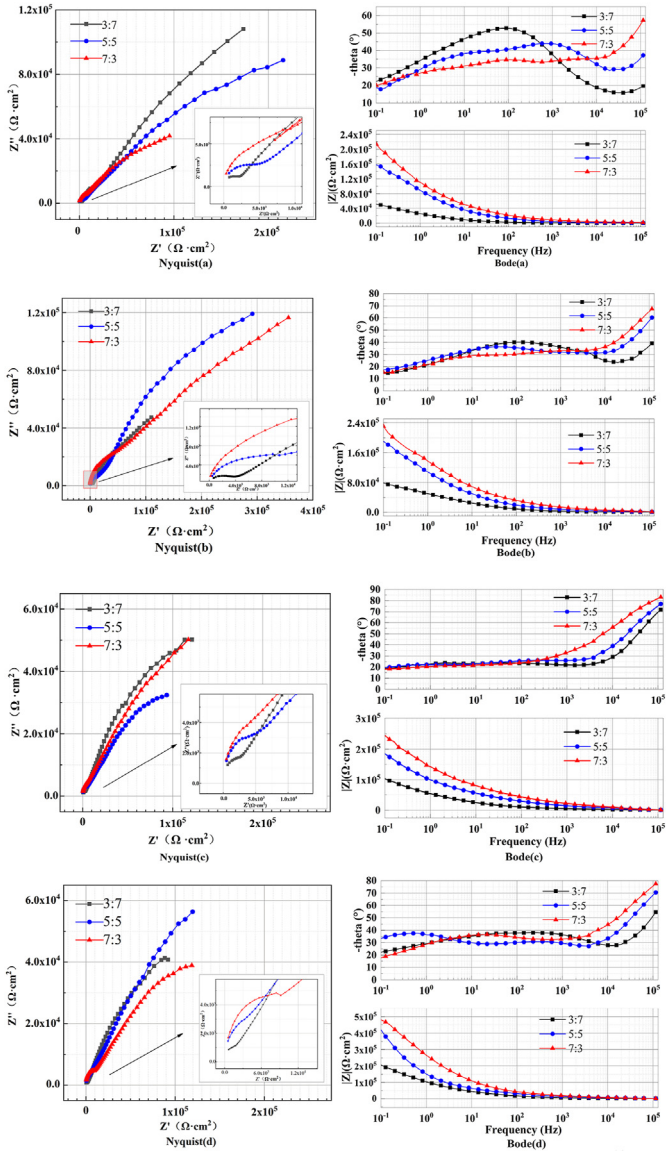

Figure 4. Nyquist and Bode diagrams of different red mud-fly ash mass ratios on the (a) 7 days, (b) 28 days, (c) 60 days and (d) 90 days.

Nyquist plots. With increasing RM mass and decreasing FA mass (i.e., increasing RM-FA ratio), the ion exchange reaction occurs and a large number of particles are formed. Under the strong adsorption of the silicon-aluminum gel formed by RM and FA hydration, free Cu^{2+} is adsorbed. Moreover, the gel and the solidified bodies are more well-connected at higher RM-FA ratios. These specimens also have lower internal porosity and denser structures, which impede charge transfer. Thus, the capacitance arc radii of the Nyquist plots increase with increasing RM-FA ratio. These Nyquist plots demonstrate that the largest capacitance arc radius is achieved when the RM-FA mass ratio is 7:3. Thus, compared with the other two RM-FA ratios, the solidified specimens produced with an RM-FA ratio of 7:3 have the densest structures and the smallest internal pores. The silicon-aluminum gel of these specimens has a strong adsorption effect and a good curing effect on the copper ions. The Bode plots of the specimens demonstrate that the impedance modulus |Z| increases with increasing RM-FA mass ratio, reaching a maximum value at a ratio of 7:3. The total impedance values of the solidified bodies positively correlate with their structural compactness. This demonstrates that the best solidified body structural compactness is achieved under an RM-FA ratio of 7:3. Moreover, the strongest copper ion solidification effect was also achieved with this ratio.

These solidified bodies are more complex than typical electrochemical systems because they are multiphase systems composed of uneven solid, liquid, and gas phases (Song, 2000). Therefore, three conductive paths exist at the beginning of the electrochemical reaction, as shown in Figure 5.

The first conductive path is the conductive path that only exists in the solid—that is, the pathway that exists in the colloid of the solidified body. This includes the hydrated and unhydrated colloid. Due to the insulation of the solidified body, impedance in the circuit is mainly provided by the solution resistance of the surrounding tiny pores. The second conductive path exists between the solid and these pores. A large amount of electric charge accumulates in the hydration gel, which causes capacitance in the pores under the action of the alternating current. Thus, circuit impedance is caused by the pore solution resistance and the capacitive reactance generated by the pore capacitance. The third conduction path is formed by the interface between the solid medium, the pores, and the pore water. Circuit impedance is caused by the pore solution resistance, the internal transfer resistance of the solid material, and the diffusion impedance. In addition, impedance at the electrode should also be considered when analyzing ion exchange at an electrode-material interface. The equivalent circuit models of the solidified bodies with different RM-FA mass ratios cured for 7, 28, 60, and 90 days were fitted by ZSimDemo software using their EIS spectra. The equivalent circuit model is R_s (Q_1 (R_{ct1}W) Q_2R_{ct2}), as shown in Figure 6.

In this model, R_s is the resistance of the solidified pore solution, R_{ct1} is the ion transfer resistance at the solid-liquid interface, R_{ct2} is the ion transfer resistance at the solidified electrode/electrode plate interface, C_1 is the capacitance of the solidified pore solution, C_2 is the capacitance at the electrode/electrode plate interface, and W is the diffusion impedance of the solidified pore solution. To further analyze the variation of pore fluid resistance R_s with varying RM-FA mass ratio, their relationship is shown in Figure 7.

The conductivity of the pore fluid is mainly controlled by the ion concentration and charge. A higher ion concentration and more highly charged ions lead to higher solution conductivity and lower pore fluid

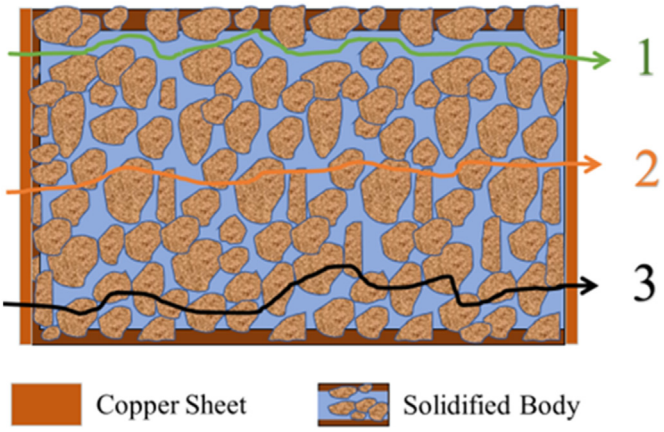

Figure 5. Schematic diagram of conductive path of solidified specimen.

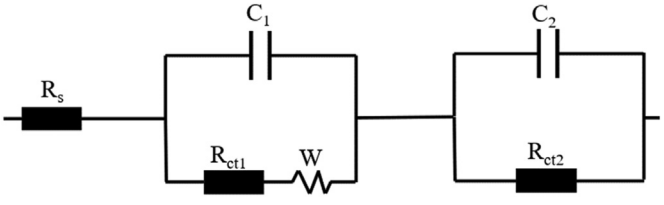

Figure 6. Equivalent circuit diagram of the solidified body.

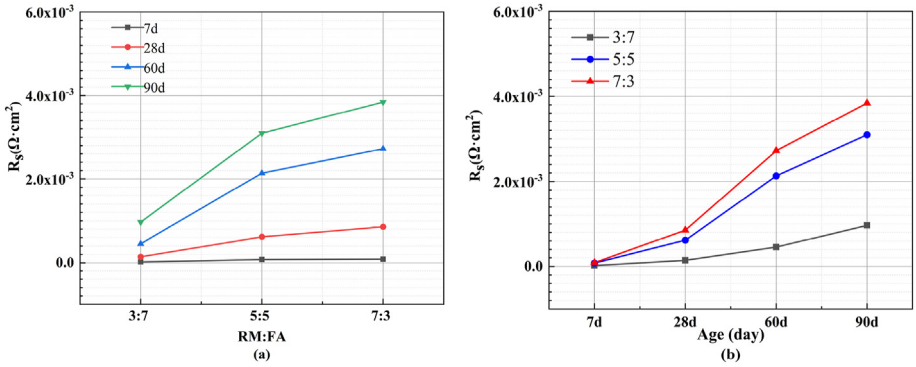

Figure 7. The change of R_s under different ratios (a) and the change of R_s under different ages.

resistance. As shown in Figure 7(a), R_s increases with increasing RM-FA mass ratio and achieves a maximum value at an RM-FA ratio of 7:3. This is because when there is less RM and more FA, more free Ca^{2+} and Cu^{2+} ions are present in the pores. Thus, the ion exchange reaction with Na^+ and K^+ in the pore solution only proceeds with difficulty. Moreover, less silicon-aluminum gel is generated by hydration at lower RM-FA ratios, and the adsorption and encapsulation of ions are weaker. The lowest R_s value is achieved with an RM-FA mass ratio of 3:7. In contrast, at higher RM-FA ratios, the solidified bodies contain more RM and less FA. Under these conditions, the hydration reaction of RM and FA is sufficient and more ion exchange occurs. The generated silicon-oxygen and aluminum-oxygen tetrahedra enhance the fixation of ions. Thus, the concentration of free high-valence ions in the pore solution decreases and the pore solution resistance increases under higher RM-FA mass ratios. The influence of curing age on the pore solution resistance R_s of the solidified specimens is shown in Figure 7(b). R_s increases with increasing curing age, and the growth rate also accelerates with increasing age. When the curing time is increased from 7 to 28 days, the growth rate of the pore fluid resistance is slow. However, this growth rate rapidly increases for curing times longer than 28 days. This is because at the early stage of curing, the hydration of RM and FA particles is relatively slow and copper ions have a certain inhibitory effect on the hydration reaction. The pores between particles are also large, and the ion concentration in the pore solution is high. However, with increasing curing age, the hydration reaction continues to proceed. The gel formed by this hydration reaction connects the particles together, and the internal structure of the solidified body gradually becomes dense (Yang et al., 2020). The pores are reduced in size and the ion concentration in the solution decreases, which increases the pore liquid resistance.

The relationship between R_{ct1} and the RM-FA mass ratio (Figure 8a) and curing age (Figure 8b) is shown in Figure 8. The charge transfer resistance also shows a trend of increasing with increasing RM-FA mass ratio. The value of R_{ct1} is very sensitive to changes in the microstructure of the solidified materials. R_{ct1} depends on the porosity of the solidified bodies and the concentration of ions in their pore solutions. When there is less RM and more FA (a low RM-FA ratio), it is difficult to activate the relatively high amount of FA, and only the activated FA reacts to form a silicon-aluminum gel. Moreover, less ion exchange occurs between Ca^{2+}/Cu^{2+} and Na^+/K^+ on the surface of RM due to the lower amount of RM (Wali et al., 2022). This leads to fewer particle clusters being formed and a lower amount of hydration gel that is not as well-connected to the solidified material. Thus, a low RM-FA ratio leads to a weaker solidification effect, larger internal pores, and easier charge transfer.

With a higher RM-FA ratio, the solidified bodies have more RM and less FM. Under these conditions, the ion exchange reaction proceeds more rapidly and forms a large number of particle clusters. Under the strong adsorption of the silica-alumina gel formed by the hydration of RM and FA, free Cu^{2+} is adsorbed and the solidified body components form stronger connections. Moreover, the solidified bodies have lower internal porosity and denser structures, which makes charge transfer difficult. Therefore, R_{ct1} increases with increasing RM-FA mass ratio.

3.2. *Unconfined compressive strengths of RM-FA cured bodies under different RM-FA ratios*

UCS tests were performed to evaluate the degree of curing in the solidified bodies. Clearly, the RM-FA ratio and the curing age significantly influence the compressive strengths of these solidified bodies.

To clearly characterize the changes in the solidified body strengths, their UCS values under different RM-FA mass ratios were plotted, as shown in Figure 9(a). With increasing RM content (and increasing RM-FA ratio), the FA content decreases and the UCS values of the solidified bodies increase. The highest solidified body strength is achieved with an

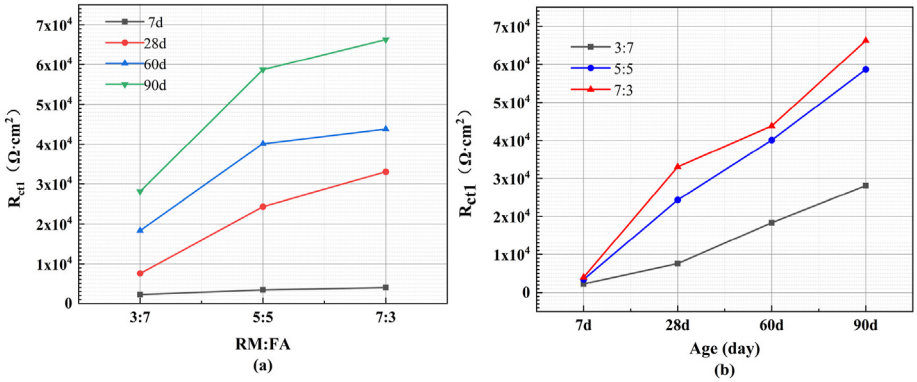

Figure 8. (a) the change of R_{ct1} under different ratios (b) the change of R_{ct1} under different ages.

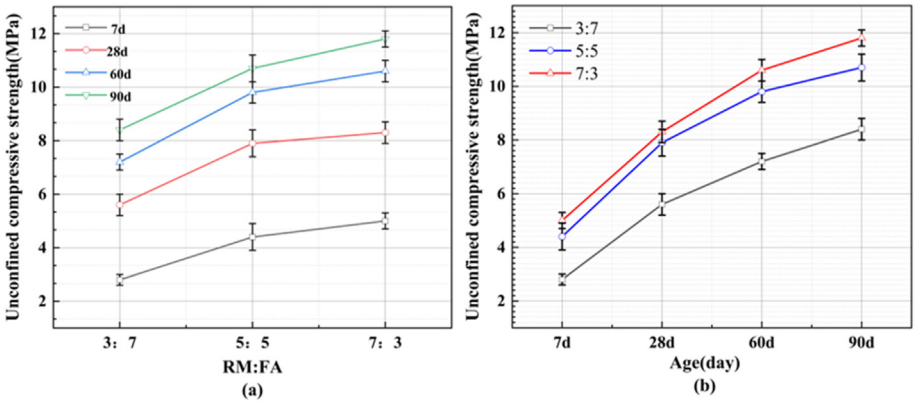

Figure 9. (a) the change of unconfined compressive strength under different ratios (b) the change of unconfined compressive strength under different ages.

RM-FA mass ratio of 7:3. This higher UCS is due to the higher OH^- ion concentration in the copper-contaminated soil after the addition of RM, FA, cement, and CaO. These OH^- ions can react with Cu^{2+} to form copper hydroxide. Some copper ions exist in the form of precipitates. When the content of free copper ions in the soil decreases, precipitation fills the internal pores of the solidified bodies and densifies their structures. This precipitation process is a series of chemical reactions. Aluminosilicate, the main mineral component of RM, has hydraulic cementation properties under the action of the activator.

FA particles are mainly composed of SiO_2–Al_2O_3 vitreous bodies with varying sizes and a small number of carbon particles. The SiO_2–Al_2O_3 vitreous bodies are composed of irregular porous single beads, continuous beads, and sponge-like bodies. FA particles with higher vitreous content also have higher activity. The small active SiO_2 particles react with Al_2O_3 in alkaline environments by a depolymerization-condensation reaction (Yin et al., 2018). That is, the aluminosilicate solids in FA dissolve and depolymerize into oligomer-silica tetrahedral SiO_4 and alumina tetrahedral AlO_4. At the same time, silicon-aluminum hydrate gel is formed on the surface of the vitreous bodies. As the aluminosilicate solids continuously dissolve and depolymerize and the hydrate gel forms, the gel diffuses from the surface of the vitreous bodies to their internal pores and cracks. Here, polycondensation occurs, and the gel becomes denser. When RM and FA are used to solidify copper ion-contaminated soil, the activities of RM and FA are enhanced by increasing the RM-FA mass ratio and due to the synergistic effect of CaO and cement. The silicon-aluminum gel formed by hydrolysis and the hydration reaction can solidify Cu^{2+}. At the same time, the gel densifies the solid structure, the strength of the solidified body increases, and the UCS of the solidified body also increases.

The UCS values of the solidified bodies also show an increasing trend with increasing curing age, as shown in Figure 9(b). In the early stage of the solidification, the hydration reaction between RM and FA only slowly progresses, and the solidified body strength is provided by the hydration product of cement. More RM and FA particles exist in their original state, and Cu^{2+} in the soil inhibits the hydration reaction. Thus, the strengths of the solidified bodies are lower after short curing times. However, as the curing age increases, the activities of RM and FA are stimulated. Moreover, the hydration reaction and ion exchange reaction fully proceed. The silica-alumina hydrate gel formed by the hydration of RM, the silica-alumina hydrate gel formed by the hydration of FA, the silicon-oxygen tetrahedral SiO_4, and the aluminum-oxygen tetrahedral AlO_4 all contribute to strength in the later stage of curing. Additionally, the pores in the solid system are filled with hydration products, Cu^{2+} solidification is enhanced, and the structural strength of the cured solidified system is also enhanced. At this time, the growth rate gradually slows down. Figure 9(b) also demonstrates that when the RM-FA ratio is 7:3, the relationship curve between the two variables is on the top side. This is a clear, intuitive indication that the solidification of Cu^{2+}-contaminated soil is optimized with an RM-FA ratio of 7:3.

In summary, the pore liquid resistance R_s and the UCS q_u of the solidified bodies both increase with increasing RM-FA mass ratio as well as with increasing curing age. The strength of these solidified bodies is related to their composition and morphology. With increasing RM-FA mass ratio and age, a large number of cementitious products are generated in the internal structure of the solidified bodies. Thus, an increasing amount of cementitious products are formed between particles. The resulting mixture of CSH gel and Aft minerals fills the pores of the particles, resulting in lower internal porosity and a less well-developed pore network. This leads to enhanced strength. Moreover, pore solution gradually increases with increasing strength, demonstrating the existence of a correlation between these two values. By fitting these obtained test values, the relationship between UCS and pore liquid resistance can be established by fitting R_s as the abscissa and q_u as the ordinate. A logarithmic relationship was used to fit the R_s and strength values, as shown in Figure 10. The relationship and correlation obtained by fitting are shown in Eq. (2). The high R^2 value demonstrates the high accuracy of this logarithmic relationship. Therefore, strength can be quantitatively predicted by determining R_s, which can be used to evaluate the degree of curing in solidified bodies. This demonstrates the effectiveness and convenience of using EIS as a non-destructive technique for analyzing the solidification of contaminated soil.

$$q_u = 1.55\ln(R_s) + 19.38, R^2 = 0.9776 \quad (2)$$

The charge transfer resistance R_{ct1} and pore liquid resistance R_s also show a trend of increasing with increasing RM-FA mass ratio and curing

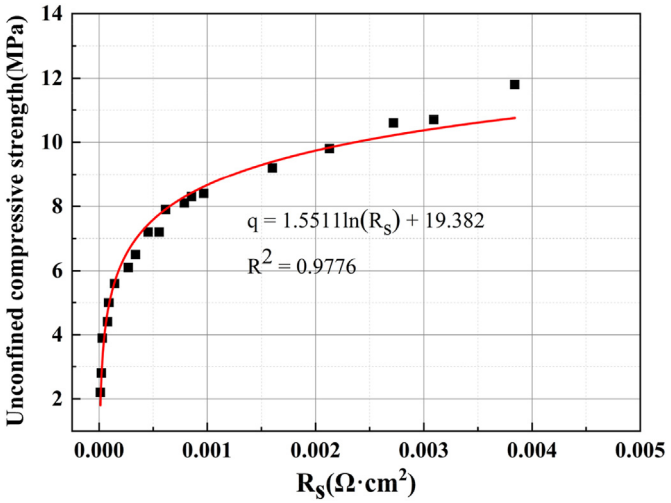

Figure 10. The logarithmic fit of Rs and intensity.

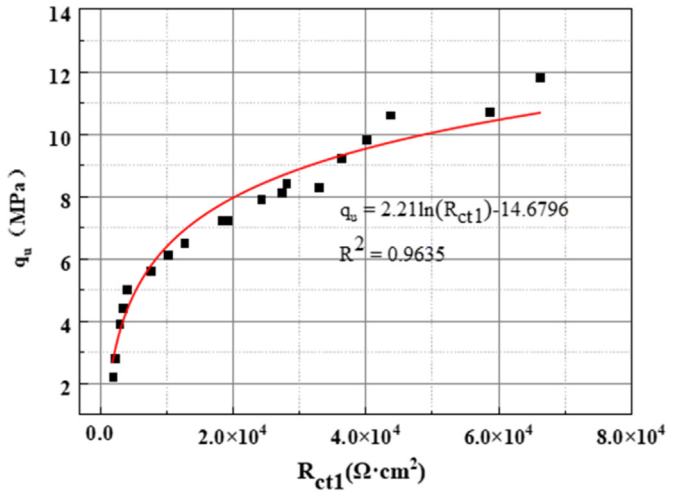

Figure 11. The logarithmic fit of R_{ct1} and intensity.

age. This is consistent with the UCS trend. Through the same fitting method, the obtained test values were fitted with R_{ct1} as the abscissa and q_u as the ordinate to establish the relationship between the UCS and the ion transfer resistance at the solid-liquid interface. This logarithmic relationship is shown in Figure 11 and Eq. (3). A positive correlation exists between R_{ct1} and UCS, and the R^2 value is 0.9635. Therefore, the relationship between R_{ct1} and UCS can also be used to quantitatively predict solidified body strength and evaluate the degree of curing.

$$q_u = 2.21\ln(R_{ct1}) - 14.6797,\ \ R^2 = 0.9635 \tag{3}$$

This analysis demonstrates that the electrochemical impedance parameters R_s and R_{ct1} have a certain correlation with the strength of the solidified bodies. R_{ct1} has a stronger linear correlation with the strength compared with R_s. Moreover, the radius of the capacitance arc in the Nyquist plot's high-frequency region reflects the magnitude of R_{ct1} to a certain extent. Therefore, changes in strength can be qualitatively determined by EIS. The parameter R_{ct1} can be obtained by equivalent circuit fitting, which can quantitatively predict the strength and evaluate the degree of curing effect of these solidified bodies.

3.3. Microstructural characteristics of solidified bodies under different RM-FA ratios

SEM was used to investigate the microstructural morphologies of the hydration products in the solidified bodies. This was done to analyze the solidification effect of the RM-FA-cement-lime system on the copper ions in these specimens. Figure 12 shows SEM images of the solidified specimens produced with different RM-FA mass ratios after 90 days of curing.

Comparing these specimens, it is clear that a denser structure is obtained with increasing RM-FA mass ratio. In a strong alkaline environment, finer solid particles more easily adhere to the surfaces of larger particles (Bai et al., 2017; Nie et al., 2020), As shown in Figure 12(a), when the mass ratio of RM-FA is 3:7, the gel particles are relatively dispersed, there are large pores between the particle clusters, and the needle bar gel is also adhered to the exterior of these particle groups. When the RM-FA mass ratio is 5:5, as shown in Figure 12(b), the gel particle clusters are less widely dispersed and display significantly reduced porosity. Some gel is formed inside the system, and this gel strongly adsorbs ions. Thus, the surrounding particle clusters are denser and have a large specific surface area. As shown in Figure 12(c), when the mass ratio of RM-FA is 7:3, a very dense cage-like gel forms inside the solidified body. The gel is tightly connected, and a large number of needle-like gel particles are attached to the exterior of the cage-like gel (Wang et al., 2020). These needle-like gel particles help stabilize the gel

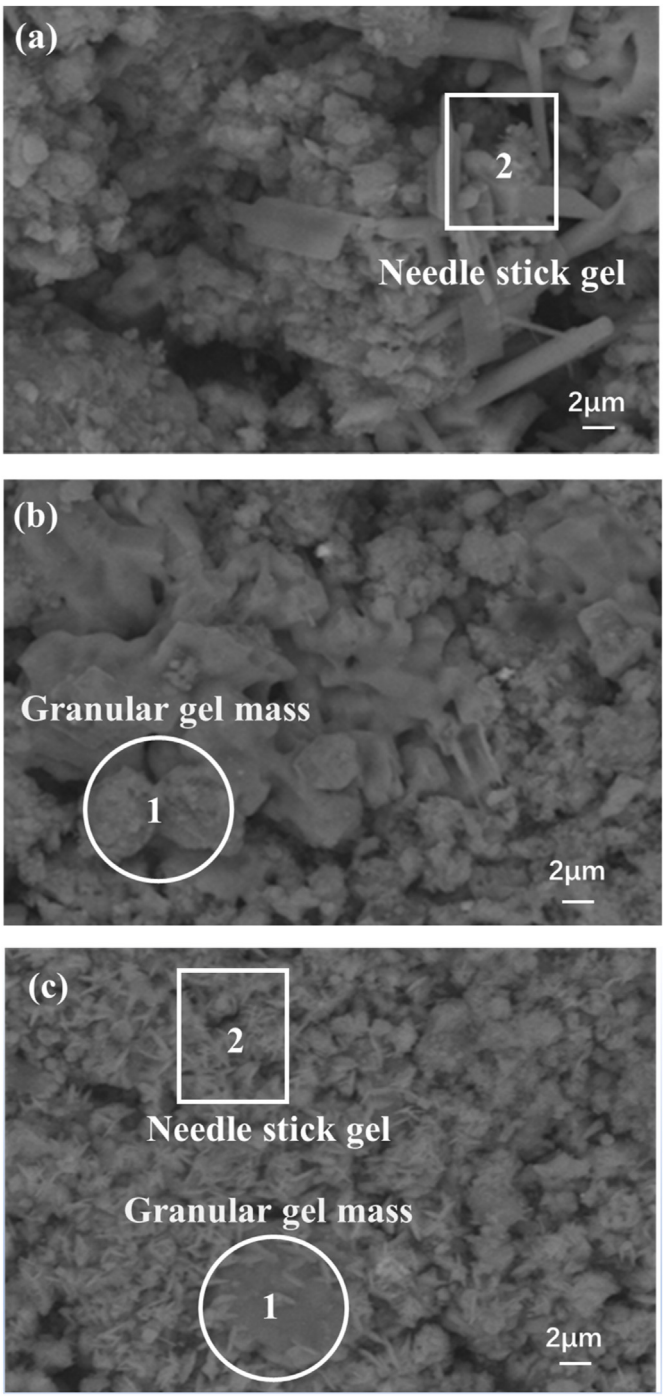

Figure 12. Microscopic images of solidified bodies with red mud-fly ash mass ratios of (a) 3:7, (b) 5:5, and (c) 7:3 after 90 days.

structure and enhance the curing of copper ions. Overall, this analysis demonstrates that the microstructural characteristics of the cured specimens are consistent with the variation of EIS parameters with changing RM-FA mass ratio. This SEM analysis is further evidence that the degree of curing is enhanced by increasing the RM-FA mass ratio. Moreover, these SEM images reveal the microscopic mechanism of the solidification of copper ion-contaminated soil by the RM-FA-cement-lime system.

4. Conclusions

According to the results presented herein, the following main conclusions can be drawn:

(1) EIS analysis of the solidified bodies obtained using different RM-FA mass ratios demonstrates that their Nyquist plots increase with increasing RM-FA mass ratio. Moreover, the capacitive arc radii of these Nyquist plots also increase with increasing RM-FA mass ratio. The largest capacitive reactance arc radius is obtained with an RM-FA mass ratio of 7:3. The impedance modulus values |Z| in the Bode plots also increase with increasing RM-FA mass ratio, with the highest |Z| value also obtained with an RM-FA mass ratio of 7:3.

(2) The electrochemical impedance spectra of the cured bodies were fitted to determine that the equivalent circuit model of these cured bodies is R_s (Q_1 (R_{ct1}W) Q_2R_{ct2}). Experimental results demonstrated that the pore solution resistance R_s increases with increasing RM-FA mass ratio and the number of curing days. Additionally, the growth rate of R_s significantly accelerates with increasing curing time. The relationship between the solid-liquid interface ion transfer resistance R_{ct1} and curing time is similar to that with R_s. The highest R_s and R_{ct1} values are both obtained after curing for 90 days with an RM-FA mass ratio of 7:3.

(3) UCS tests were performed to analyze the relationship between the RM-FA mass ratio and strength as well as the relationship between strength and the values of R_s and R_{ct1}. The UCS values of the cured specimens increase with increasing RM-FA mass ratio and age, but the UCS growth rate decreases with increasing age. The highest UCS is achieved with an RM-FA mass ratio of 7:3. By using logarithmic relationship fitting, R_s and R_{ct1} show very good positive correlations with strength, indicating that the strength characteristics of these cured bodies can be evaluated by EIS.

(4) SEM analysis of the solidified bodies demonstrated that when the mass ratio of RM-FA is 7:3, the hydration products formed inside the solidified body have a stable and dense structure as well as small internal pores. Moreover, the solidification effect on the copper ions is the strongest under this RM-FA ratio. The microstructure characteristics of the solidified specimens are consistent with the variation of electrochemical impedance parameters, further verifying the feasibility of using EIS to reveal the solidification mechanism of Cu^{2+}-contaminated soil.

Declarations

Author contribution statement

Wang Wen; Lijun Jia; Jun Xie; Funan Sun: Conceived and designed the experiments; Performed the experiments; Analyzed and interpreted the data; Wrote the paper.

Bin He; Pengju Han; Xiaohong Bai: Conceived and designed the experiments; Analyzed and interpreted the data.

Wenjing Zhao; Huimin Feng; Dehua Cao: Contributed reagents, materials, analysis tools or data.

Funding statement

Prof. Bin He was supported by National Natural Science Foundation of China [41807256, 51208333].

Data availability statement

Data will be made available on request.

Declaration of interest's statement

The authors declare no conflict of interest.

Additional information

No additional information is available for this paper.

References

Atanes, E., Cuesta-Garcia, B., Nieto-Marquez, A., Fernandez-Martinez, F., 2019. A mixed separation-immobilization method for soluble salts removal and stabilization of heavy metals in municipal solid waste incineration fly ash. J. Environ. Manag. 240, 359–367.

Bai, B., Long, F., Rao, D., Xu, T., 2017. The effect of temperature on the seepage transport of suspended particles in a porous medium. Hydrol. Process. 31, 382–393.

Casero, E., Parra-Alfambra, A.M., Petit-Domínguez, M.D., Pariente, F., Lorenzo, E., Alonso, C., 2012. Differentiation between graphene oxide and reduced graphene by electrochemical impedance spectroscopy (EIS). Electrochem. Commun. 20, 63–66.

Cho, D.W., Yoon, K., Ahn, Y., Sun, Y., Tsang, D.C.W., Hou, D., Ok, Y.S., Song, H., 2019. Fabrication and environmental applications of multifunctional mixed metal-biochar composites (MMBC) from red mud and lignin wastes. J. Hazard Mater. 374, 412–419.

Derakhshan Nejad, Z., Jung, M.C., Kim, K.H., 2018. Remediation of soils contaminated with heavy metals with an emphasis on immobilization technology. Environ. Geochem. Health 40, 927–953.

Dong, B., Zhang, J., Liu, Y., Fang, G., Ding, Z., Xing, F., 2016. Tracing hydration feature of aluminophosphate cementitious materials by means of electrochemical impedance method. Construct. Build. Mater. 113, 997–1006.

Du, J., Zheng, G., Liu, B., Jiang, N.-J., Hu, J., 2020. Triaxial behavior of cement-stabilized organic matter–disseminated sand. Acta Geotech 16, 211–220.

Duan, Q., Lee, J., Liu, Y., Chen, H., Hu, H., 2016. Distribution of heavy metal pollution in surface soil samples in China: a graphical review. Bull. Environ. Contam. Toxicol. 97, 303–309.

Fang, Y., Li, H., Wang, Z., Zhang, K., Cui, P., Dong, B., 2019. The effect of metakaolin on the hardening process of alkali activated slag by using electrochemical impedance spectroscopy. IOP Conf. Ser. Earth Environ. Sci. 300.

Garau, G., Castaldi, P., Santona, L., Deiana, P., Melis, P., 2007. Influence of red mud, zeolite and lime on heavy metal immobilization, culturable heterotrophic microbial populations and enzyme activities in a contaminated soil. Geoderma 142, 47–57.

Gong, Y., Zhao, D., Wang, Q., 2018. An overview of field-scale studies on remediation of soil contaminated with heavy metals and metalloids: technical progress over the last decade. Water Res. 147, 440–460.

Goodarzi, A.R., Movahedrad, M., 2017. Stabilization/solidification of zinc-contaminated kaolin clay using ground granulated blast-furnace slag and different types of activators. Appl. Geochem. 81, 155–165.

Hossain, M.U., Wang, L., Chen, L., Tsang, D.C.W., Ng, S.T., Poon, C.S., Mechtcherine, V., 2020. Evaluating the environmental impacts of stabilization and solidification technologies for managing hazardous wastes through life cycle assessment: a case study of Hong Kong. Environ. Int. 145, 106139.

Hu, B., Shao, S., Fu, Z., Li, Y., Ni, H., Chen, S., Zhou, Y., Jin, B., Shi, Z., 2019. Identifying heavy metal pollution hot spots in soil-rice systems: a case study in South of Yangtze River Delta, China. Sci. Total Environ. 658, 614–625.

Hua, Y., Heal, K.V., Friesl-Hanl, W., 2017. The use of red mud as an immobiliser for metal/metalloid-contaminated soil: a review. J. Hazard Mater. 325, 17–30.

Huang, J., 2018. Diffusion impedance of electroactive materials, electrolytic solutions and porous electrodes: Warburg impedance and beyond. Electrochim. Acta 281, 170–188.

Kirgiz, M.S., 2018. Pulverized fuel ash cement activated by nanographite. ACI Mater. J. 115.

Kumar, A., Kumar, S., 2013. Development of paving blocks from synergistic use of red mud and fly ash using geopolymerization. Construct. Build. Mater. 38, 865–871.

Li, W., Ni, P., Yi, Y., 2019. Comparison of reactive magnesia, quick lime, and ordinary Portland cement for stabilization/solidification of heavy metal-contaminated soils. Sci. Total Environ.z 671, 741–753.

Liu, H., Yang, H., Yi, F., 2016. Experimental study of the complex resistivity and dielectric constant of chrome-contaminated soil. J. Appl. Geophys. 131, 109–116.

Liu, L., Li, W., Song, W., Guo, M., 2018. Remediation techniques for heavy metal-contaminated soils: principles and applicability. Sci. Total Environ. 633, 206–219.

Mahendran, V., Philip, J., 2013. Sensing of biologically important cations such as Na^+, K^+, Ca^{2+}, Cu^{2+}, and Fe^{3+} using magnetic nanoemulsions. Langmuir 29 (13), 4252–4258.

Nie, Q., Li, Y., Wang, G., Bai, B., 2020. Physicochemical and microstructural properties of red muds under acidic and alkaline conditions. Appl. Sci. 10.

Qiu, Q., Gu, Z., Xiang, J., Huang, C., Hong, S., Xing, F., Dong, B., 2017. Influence of slag incorporation on electrochemical behavior of carbonated cement. Construct. Build. Mater. 147, 661–668.

Song, G., 2000. Equivalent circuit model for AC electrochemical impedance spectroscopy of concrete. Cement Concr. Res. 30 (11), 1723–1730.

Suo, C., Fang, P., Cao, H., Cao, J., Liu, K., Dong, X., 2021. Influence and microscopic mechanism of the solid waste-mixture on solidification of Cu^{2+}-contaminated soil. Construct. Build. Mater. 305, 124651.

Tajudin, S.A.A., Azmi, M.A.M., Nabila, A.T.A., 2016. Stabilization/solidification remediation method for contaminated soil: a review. IOP Conf. Ser. Mater. Sci. Eng. 136.

Tian, Y., Ning, X.N., Liu, J.Y., Zhou, J.B., Yang, Z.Y., Li, L., 2011. Study on the Solidification/stabilization Treatment of Tannery Sludge, International Conference on Energy, Environment and Sustainable Development (ICEESD 2011). Trans Tech Publications Ltd, Shanghai Univ Elect Power, Shanghai, PEOPLES R CHINA, pp. 1951–1954.

Viyasun, K., Anuradha, R., Thangapandi, K., Santhosh Kumar, D., Sivakrishna, A., Gobinath, R., 2021. Investigation on performance of red mud based concrete. Mater. Today Proc. 39, 796–799.

Wali, S.U., Alias, N.B., Harun, S.B., Umar, K.J., Gada, M.A., Dankani, I.M., Usman, A.A., 2022. Water Quality Indices and Multivariate Statistical Analysis of Urban

Groundwater in Semi-arid Sokoto basin, Northwestern Nigeria. Groundwater Sustainable Dev, 100779.
Wang, D., Wang, H., Larsson, S., Benzerzour, M., Maherzi, W., Amar, M., 2020. Effect of basalt fiber inclusion on the mechanical properties and microstructure of cement-solidified kaolinite. Construct. Build. Mater. 241, 118085.
Wang, F., Wang, H., Al-Tabbaa, A., 2015. Time-dependent performance of soil mix technology stabilized/solidified contaminated site soils. J. Hazard Mater. 286, 503–508.
Wang, H., Zentar, R., Wang, D., Ouendi, F., 2022. New applications of ordinary Portland and calcium sulfoaluminate composite binder for recycling dredged marine sediments as road materials. Int. J. GeoMech. 22 (6), 04022068.
Xia, W.Y., Du, Y.J., Li, F.S., Li, C.P., Yan, X.L., Arulrajah, A., Wang, F., Song, D.J., 2019. In-situ solidification/stabilization of heavy metals contaminated site soil using a dry jet mixing method and new hydroxyapatite based binder. J. Hazard Mater. 369, 353–361.
Yang, Y.X., Li, H., Zheng, W.K., Bai, Y., Liu, Z.M., Zhang, J.J., 2019. Experimental study on calcining process of secondary coated ceramsite solidified chromium contaminated soil. Sci. Adv. Mater. 11, 208–214.
Yang, Z., Li, X., Li, D., Wang, Y., Liu, X., 2020. Effects of long-term repeated freeze-thaw cycles on the engineering properties of compound solidified/stabilized Pb-contaminated soil: deterioration characteristics and mechanisms. Int. J. Environ. Res. Publ. Health 17 (5), 1798.
Yin, B., Kang, T., Kang, J., Chen, Y., 2018. Analysis of active ion-leaching behavior and the reaction mechanism during alkali activation of low-calcium fly ash. Int. J. Concr. Struct. Mater. 12.
Younsi, A., Aït-Mokhtar, A., Hamami, A.A., 2015. Investigation of some electrochemical phenomena induced during chloride migration test on cementitious materials. Eur. J. Environ. Civ. Eng. 21, 303–318.
Zentar, R., Wang, H., Wang, D., 2021. Comparative study of stabilization/solidification of dredged sediments with ordinary Portland cement and calcium sulfo-aluminate cement in the framework of valorization in road construction material. Construct. Build. Mater. 279, 122447.
Zha, F.S., Liu, S.Y., Du, Y.J., Cui, K.R., 2007. The electrical resistivity characteristics of unsaturated clayey Soil. Rock Soil Mech. 28 (8), 1671–1676.
Zha, F.S., Liu, S.Y., Du, Y.J., Cui, K.R., 2009. Evaluation of physicochemical process in stabilized expansive soils using electrical resistivity method. Rock Soil Mech. 30 (6), 1711–1718.
Zha, F.S., Liu, S.Y., Du, Y.J., Cui, K.R., 2011. Characteristics of electrical resistivity of compacted loess. Rock Soil Mech. 32 (S2), 155–158.
Zha, F.S., Liu, J.j., Xu, L., Deng, Y.S., Yang, C.B., Chu, C.F., 2019. Electrical resistivity of heavy metal contaminated soils solidified/stabilized with cement-fly ash. Rock Soil Mech. 40 (12), 9.